

# Two Improved Forensic Methods of Detecting Contrast Enhancement in Digital Images

Xufeng Lin, Xingjie Wei and Chang-Tsun Li

Department of Computer Science, University of Warwick, Coventry, CV4 7AL, UK  
{xufeng.lin, x.wei, c-t.li}@warwick.ac.uk

## ABSTRACT

Contrast enhancements, such as histogram equalization or gamma correction, are widely used by malicious attackers to conceal the cut-and-paste trails in doctored images. Therefore, detecting the traces left by contrast enhancements can be an effective way of exposing cut-and-paste image forgery. In this work, two improved forensic methods of detecting contrast enhancement in digital images are put forward. More specifically, the first method uses a quadratic weighting function rather than a simple cut-off frequency to measure the histogram distortion introduced by contrast enhancements, meanwhile the averaged high-frequency energy measure of histogram is replaced by the ratio taken up by the high-frequency components in the histogram spectrum. While the second improvement is achieved by applying a linear-threshold strategy to get around the sensitivity of threshold selection. Compared with their original counterparts, these two methods both achieve better performance in terms of ROC curves and real-world cut-and-paste image forgeries. The effectiveness and improvement of the two proposed algorithms are experimentally validated on natural color images captured by commercial camera.

**Keywords:** Digital forensics, contrast enhancement detection, inter-channel similarity

## 1. INTRODUCTION

In a typical cut-and-paste image forgery scene, the contrast between the background and the pasted region is usually not as consistent as that of the original image due to varying lighting conditions. Therefore, to avoid detection, the cut-and-paste image forgery is usually covered up by some contrast enhancement operations after one image is forged. However, the more one tries to hide, the more is exposed. Most of the contrast enhancements are implemented by intensity mapping operation which introduces some statistical traces that can be used to expose cut-and-paste image forgery. For example, a blind method is proposed in [1] to detect globally and locally applied contrast enhancement operations. It is based on the observation that contrast enhancement will introduce sudden peaks and zeros in the histogram and therefore increase high-frequency components in the histogram spectrum. To track down the footprints of contrast enhancement, a high-frequency measurement of histogram spectrum  $F$  is constructed and subsequently compared with a threshold  $\eta$ . A value of  $F$  greater than  $\eta$  signifies the detection of contrast enhancement.

Although good results are achieved, it is not convenient to use in practice as some parameters need to be determined by users, such as the cut-off frequency  $T$ . The optimal parameters may vary with different forms of contrast enhancements. What is more, for small image blocks, the statistical significance of the calculated histogram would be reduced, so its capability of detecting small blocks is limited. Most importantly, as the histogram of image can be easily tampered, this kind of histogram-based forensic methods will fail if the traces left on the image histogram have been concealed by attackers. For example, Cao et al. used a local random dithering technique to remove the peak and gap artifacts of histogram introduced by contrast enhancements.<sup>2</sup> Essentially, they added Gaussian noise with appropriate variance onto the contrast enhanced image to smooth the histogram and therefore conceal the high-frequency abnormality. In [3], M. Barni et al. proposed a universal technique to hide the traces of histogram-based image manipulations. For a manipulated image with histogram  $h_y$ , they first found the most similar histogram  $h_x$  from a reference histogram database, according to which a displacement matrix is obtained by solving a mixed integer nonlinear problem (MINLP). The displacement matrix then is involved in a pixel remapping process so as to bring  $h_y$  close to  $h_x$  while keeping the image distortion

as low as possible. For these reasons, we proposed a novel forensic method of detecting contrast enhancement using the inter-channel similarity of high-frequency components.<sup>4</sup> The motivation of our work is that linear or non-linear contrast enhancements will disturb the inter-channel high-frequency components similarity introduced by color filter array (CFA) interpolation in most commercial digital cameras. An inter-channel high-frequency similarity measurement  $S$  is therefore proposed for detecting contrast enhancements. This method is more capable of localizing tampered regions and has good robustness against some state-of-the-art histogram-based anti-forensic schemes.<sup>2,3</sup> But it may fail if the image block in question 1) does not contain enough or 2) too much high-frequency content to provide trustworthy evidence. Given that the methods reported in [1] and [4] have their pros and cons, in this work we propose two improved algorithms with respect to these two approaches.

The rest of paper is organized as follows. In Section 2, we first review the original algorithms and list out some shortcomings that will be addressed in this paper. Then we come up with the details of the improved counterparts accordingly. In the following Section 3, experiments are setup to confirm the merits of the proposed approaches with detailed analysis and a comparison to prior methods in terms of both ROC curves and real-world cut-and-paste image forgeries. Finally, Section 4 concludes this paper.

## 2. PROPOSED METHODOLOGIES

### 2.1 Contrast Enhancement Detection Based on Histogram

Due to observational noise,<sup>5</sup> sampling effects, complex lighting environments and CFA interpolation, the histograms of natural images are strongly lowpass and do not contain sudden zeros or impulsive peaks. While the smoothness of the original histogram will get disturbed or destroyed by contrast enhancement manipulations, which consequently cause the increase of high-frequency energy in the histogram spectrum. Based on this observation, Stamm and Liu proposed a general contrast enhancement detection algorithm as follows:<sup>1</sup>

- Step 1. Obtain the image's histogram  $h(x)$  and calculate the modified histogram  $g(x)$  as follows:

$$g(x) = h(x)p(x) \quad (1)$$

where  $x$  is the original pixel value, and  $p(x)$  is a pinch off function, whose role is to eliminate the low-end or high-end saturated effect in images:

$$p(x) = \begin{cases} \frac{1}{2} \left( 1 - \cos\left(\frac{\pi x}{N_p}\right) \right), & x \leq N_p \\ \frac{1}{2} \left( 1 + \cos\left(\frac{\pi(x+N_p-255)}{N_p}\right) \right), & x \geq 255 - N_p \\ 1, & \text{else} \end{cases} \quad (2)$$

$N_p$  is the width of the region in histogram spectrum over which  $p(x)$  decays from 1 to 0. Usually it is set to be around 8.

- Step 2. Transform  $g(x)$  into the discrete Fourier frequency domain,  $G(k)$ , and calculate the high-frequency measurement  $F$  according to

$$F = \frac{1}{N} \sum_k |\beta(k)G(k)|, k = 0, 1, \dots, 255 \quad (3)$$

where  $N$  is the total number of pixels, and  $\beta(k)$  is the cut-off function deemphasizing the low-frequency components of  $G(k)$ :

$$\beta(k) = \begin{cases} 1, T \leq k \leq 255 - T \\ 0, \text{else} \end{cases} \quad (4)$$

where  $T$  corresponds to a desired cut-off frequency.

- Step 3.  $F$  is compared with a threshold  $\eta$  to determine whether a contrast enhancement has been applied. Locally applied contrast enhancement can be discovered by blockwisely performing the above procedures.

As can be seen from the above steps, there are some parameters or switches that need to be set carefully by users. The first one is  $N_p$ , which controls the width of the region of interest in the frequency spectrum. Setting it to be a small value around 8 eliminates the saturated effects, and meanwhile preserves the spectrum information as much as possible. The next parameter needs to be considered is the cut-off frequency  $T$ , which can be viewed as the dividing line between the low-frequency and high-frequency region. It is an important parameter as it directly affects the calculation of the averaged high-frequency measurement  $F$ . A large  $T$  means that only a small proportion of high-frequency components are taken into account, which gives rise to the over-sensitiveness of detector for a fixed threshold. On the other hand, a small  $T$  may incorporate some undesired low-frequency components into the calculation and hence bring the detection accuracy down. For one specific contrast enhancement algorithm with fixed parameters, we can analytically or experimentally determine the optimal  $T$  for detection. But unfortunately, we do not have any prior information about the image being tested, and the optimal  $T$  varies from different forms of contrast enhancements. This can be demonstrated by the example of linear enhancement, which has the form of:

$$Q(x) = \left[ \frac{p}{q}x \right] \quad (5)$$

where  $x$  is the original pixel value,  $[\cdot]$  is a rounding operation, and  $p, q$  are two integers which have already been divided by their greatest common divisor. This linear mapping function expands every  $q$  bins into  $p$  bins in the histogram in case  $p > q$ , while combines every  $q$  histogram bins to produce  $p$  bins in the other case  $p < q$ . But in either case, the histogram of the new image has a period of  $p$ . As a result, peaks appear at the frequencies  $\frac{2\pi i}{p}, i = 1, 2, \dots, p-1$  in the spectrum of histogram. As shown in Figure 1, for a fixed cut-off frequency  $T$ , it works well for  $p = 7, q = 5$ , because the increase of high-frequency components in the histogram spectrum has been captured in the regions bounded by  $T$ . However, the same  $T$  fails for the case  $p = 3, q = 10$  since the peaks caused by the linear transformation coincidentally fall outside the bounded region. Notice that the zero-frequency component of the histogram spectrum has been shifted to the center for better visualization. Hence, one can see that it is hard to determine an optimal  $T$  for all kinds of contrast enhancements unless some necessary prior information is available. Another problem of Stamm and Liu's algorithm arises from averaging the high-frequency components over the number of pixels  $N$ . As we know that the spectral energy is relevant with the variations as well as the magnitudes of the signal, so the high-frequency measure  $F$  will inevitably change dramatically with the image size and content by only considering the pixel number. The large dynamic range of  $F$  occasions the choice of threshold  $\eta$  a lot of trouble, thus we need to devise a measurement that is relatively image size and content invariant.

Based on the above analysis, we propose a new high-frequency measurement of the histogram spectrum  $E$ :

$$E = \frac{\sum_k |\omega(k)G(k)|}{\sum_k |G(k)|}, k = 0, 1, \dots, 255 \quad (6)$$

where  $\omega(k)$  is the weighting function:

$$\omega(k) = \left( \frac{k-128}{128} \right)^2, k = 0, 1, \dots, 255 \quad (7)$$

As can be seen from Equation (6), there are two modifications of  $E$  compared with  $F$  in Equation (3): in the numerator, a quadratic weighting scheme is applied to deemphasize the low-frequency band of histogram spectrum rather than choosing a cut-off frequency  $T$ ; for the denominator, the total number of pixels  $N$  is replaced by the energy of the histogram spectrum. These simple improvements bring two substantial benefits. Firstly, we can achieve the purpose of deemphasizing the low-frequency band without choosing the optimal cut-off frequency  $T$ . Actually, it is almost impossible to find the general-purpose cut-off frequency without prior information since the optimal cut-off frequency  $T$  varies with respect to the forms and parameters of contrast enhancements. Secondly,  $E$  represents the proportion taken up by the high-frequency band in the whole histogram spectrum, therefore  $E$  remains almost invariant to image size and content. The improvements brought by these modifications will be experimentally verified in Section 3.

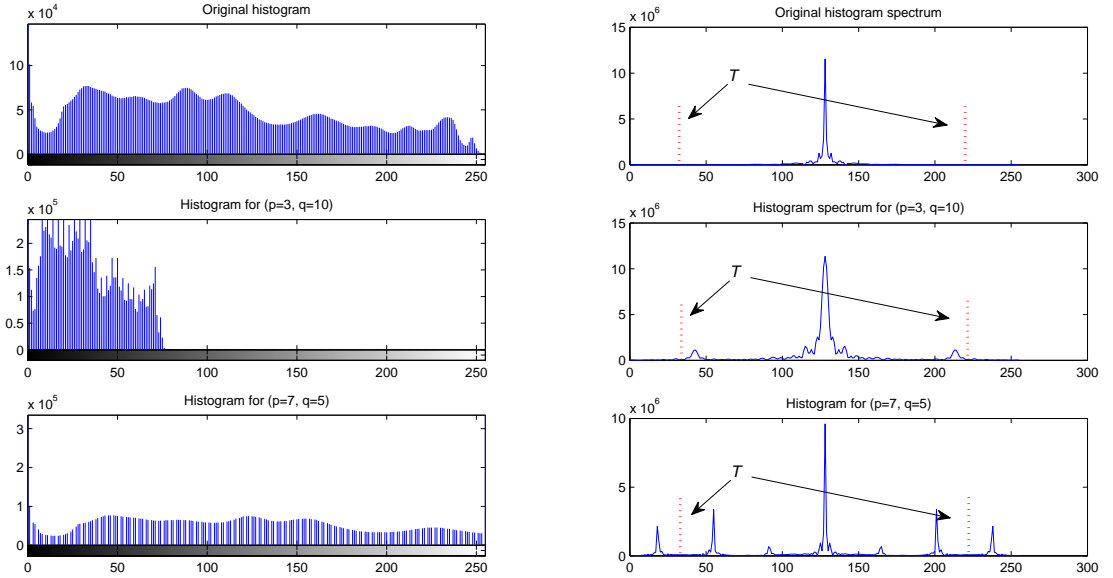


Figure 1: The choice of cut-off frequency  $T$

## 2.2 Contrast Enhancement Detection Based on Inter-channel Similarity

For the sake of completeness, we will first review the algorithm described in [4]. In the imaging process of most commercial cameras, a CFA is placed before the sensor to capture one of the three primary colors for each pixel while the other two color components are interpolated with a specific demosaicking algorithm. Human eyes are more sensitive to the green component of visible light as the peak sensitivity of the human visual system lies in the green portion of the spectrum. For this reason, most CFAs tend to sample the green channel at a higher rate than those of the red and blue channels. In the well-known Bayer CFA sampling pattern, green samples are twice as many as red and blue samples. The spectrum of green channel therefore has less aliasing and its high-frequency components are better preserved. Therefore, most of the color interpolation algorithms are based on the assumption that different color channels have similar high-frequency components. They use the high-frequency components of green channel to replace those of red and blue channels.<sup>6-8</sup>

The inter-channel similarity can be demonstrated by the constant-difference-based interpolation method (shown in Figure 2). Here we only take the reconstruction of red channel for example. Suppose  $R_s$  and  $G_s$  are the color planes sampled by the CFA. For the Bayer CFA sampling pattern, the size of  $R_s$  is only 1/4 of the image size while  $G_s$  is 1/2 of the image size. To obtain  $R_s$  and  $G_s$  with the full image size, zeros are filled at non-sample locations. Assume that  $R$  and  $G$  are color planes reconstructed from sample values  $R_s$  and  $G_s$ , respectively.  $G$  is simply reconstructed from  $G_s$  using bilinear or edge-directed interpolation. Let  $G_{sr}$  be the color plane that is produced by sampling  $G$  at red sample locations and filling in zeros at other color sample locations. The reconstruction of  $R$  then can be helped with  $G$ :

$$\begin{aligned}
 R &\approx \Psi\{R_s - G_{sr}\} + G \\
 \Rightarrow R &\approx R_l + (G - G_l) \\
 \Rightarrow R &\approx R_l + G_h
 \end{aligned} \tag{8}$$

where  $\Psi\{\cdot\}$  denotes a lowpass filter, i.e. interpolation process.  $R_l$  and  $G_l$  denote the low-frequency bands of  $R$  and  $G$ , respectively.  $G_h$  denotes the high-frequency band of  $G$ . Equation (8) can be interpreted as  $R$  ‘copies’ the high-frequency components of  $G$ .<sup>9</sup> Likewise, one can reconstruct the blue color plane  $B$ . Therefore, we get

$$R_h \approx G_h \approx B_h \tag{9}$$

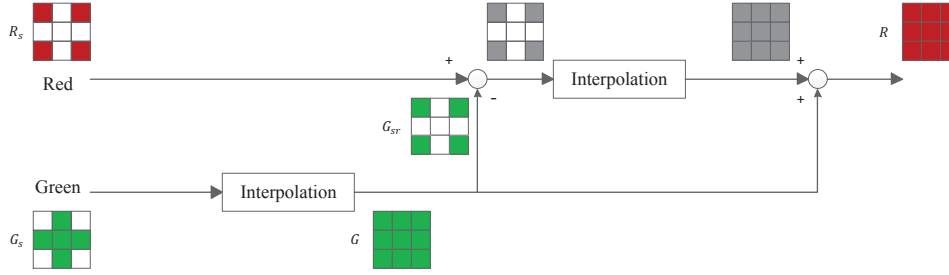


Figure 2: Constant-difference-based interpolation

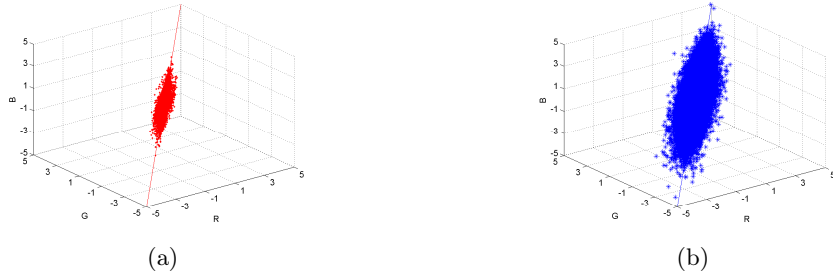


Figure 3: Scatter plots of wavelet coefficients in the diagonal subband for (a) the original images and (b) the enhanced images.

However, contrast enhancement may disturb this statistical similarity. To demonstrate this, we draw the 3D scatter plots of the averaged high-frequency wavelet coefficients for 100 original images and the corresponding enhanced images in Figure 3(a) and 3(b). The coordinates of each point denote the magnitudes of  $R$ ,  $G$  and  $B$  wavelet coefficients in diagonal subband for one image, taken at the same pixel location. In general, the points are compactly clustered along the line corresponding to vector  $[1, 1, 1]^T$  for original images, which implies the strong correlation and approximate equality of the wavelet coefficients.<sup>10</sup> For enhanced images, however, the points deviate from the line suggesting the inter-channel correlation has been reduced. Based on the above observation, we propose a metric  $S$  to measure the inter-channel high-frequency similarities:

$$S = \frac{1}{3MN} \sum_{m=0}^{M-1} \sum_{n=0}^{N-1} |D_G(m, n) - D_R(m, n)| + |D_G(m, n) - D_B(m, n)| + |D_R(m, n) - D_B(m, n)| \quad (10)$$

where  $D_R(m, n)$ ,  $D_G(m, n)$  and  $D_B(m, n)$  are the first level 2D wavelet coefficients of color channels  $R$ ,  $G$  and  $B$  in the diagonal subband.  $M$  and  $N$  are the width and height of the diagonal subband, respectively. A value of  $S$  greater than the decision threshold  $\tau$  signifies the detection of contrast enhancement. Notice that we average the inter-channel similarity measurement over three channels to make it more stable, which is slightly different from the metric proposed in [4].

The capability of detecting smaller areas usually means more accurate localization, so it is important for an image forgery detection algorithm. Inter-channel similarity based method is more capable of detecting small blocks, but it may fail when the image block 1) does not contain enough (e.g. in the all-black or all-white regions) or 2) contains too much (e.g. in the edge regions) high-frequency content. Statistically, the values of the inter-channel similarity  $S$  in Equation (10) are proportional to the means of diagonal-band wavelet coefficients. So if a hard-threshold strategy is applied, some untouched blocks in the edge regions will be incorrectly classified as enhanced ones, which will lead to the increase of false positive rate correspondingly. To solve this problem, a soft-threshold method is needed. From the experiments, the relationship between  $S$  and the mean of the wavelet coefficients  $\bar{D}$  in an untouched image is relatively stable. Therefore, we model this relationship by a linear

function and then use it in the threshold process to determine whether the image block in question is enhanced or not. If the mean of the wavelet coefficients is:

$$\bar{D} = \frac{1}{3MN} \sum_{m=0}^{M-1} \sum_{n=0}^{N-1} |D_R(m, n)| + |D_G(m, n)| + |D_B(m, n)| \quad (11)$$

where the symbols have the same meanings as in Equation (10), then the linear threshold  $\tau$  can be written as:

$$\tau = a \cdot \bar{D} + b \quad (12)$$

The relationship between  $S$  and  $\bar{D}$  relies heavily on image content, so it is difficult to exactly model it using an explicit mathematical formula. What's worse, it seems that this relationship varies from different cameras. The only useful information is that  $S$  is proportional to  $\bar{D}$  statistically. In practice, any monotone increasing expression can be applied in the thresholding, but the simplicity of linear threshold makes it advantageous when compared with other quadratic or higher power threshold.

### 3. EXPERIMENTS

#### 3.1 Experimental setup

To verify the effectiveness and improvement of the two proposed algorithms, 100 uncompressed color images (size of  $1600 \times 1200$  pixels) captured by Canon IXUS870 were used in the experiments. As in the previous works in [1–4], we will only show results for the images enhanced by power law transformation ( $\gamma$  correction):

$$\Omega(x) = \left[ 255 \left( \frac{x}{255} \right)^\gamma \right] \quad (13)$$

where  $[\cdot]$  is a rounding operation,  $\gamma$  is randomly chosen from the set  $\{0.5, 0.8, 1.5\}$ . These enhanced images were combined with the original images to create a testing database of 400 color image. To test the performance on local contrast enhancement detection, we divided each image into blocks of different sizes. For example, for blocks sized  $128 \times 128$  pixels, each image will be divided into  $\lfloor \frac{1600}{128} \rfloor \times \lfloor \frac{1200}{128} \rfloor = 108$  blocks, where  $\lfloor \cdot \rfloor$  is a floor operation.

#### 3.2 Improvement over Stamm and Liu's Method<sup>1</sup>

Let's first look at the comparison of high-frequency measurement  $F$  and  $E$  by means of changes along with block sizes. As shown in Figure 4, the average  $E$  (from 0.03 to 0.10) varies much less than the average  $F$  (from 0.06 to 0.92) when the block size is changed from  $512 \times 512$  to  $32 \times 32$  pixels. The tighter range of  $E$  makes it more stable with different block sizes, and therefore less sensitive to the threshold selection. After taking a close look at the scatter plots of  $F$  in Figure 5(a) and  $E$  in Figure 5(b), we can discover that the intra-class variation of  $E$  is much smaller than that of  $F$  (especially for the enhanced images), meanwhile the inter-class gap of  $E$  is also pulled outwards by a certain distance. The advantage becomes even more evident when the ROC curves are plotted out in Figure 6, where  $P_D$  and  $P_{FA}$  denote the true positive rate and false positive rate, respectively. The results shown in Figure 6 clearly manifest that the proposed algorithm consistently outperforms the original method with a variety of  $T$ , although the performance gain may vary with different  $\gamma$  values and block sizes. An example of real-world cut-and-paste image forgery is shown in Figure 7, where a person is cut from 7(a), then transformed using the Photoshop Curve Tools (7(d)) and pasted on 7(b) to produce the composit image in 7(c). The best detection results using algorithm in [1] and the improved counterpart are shown in Figure 8(a) and 8(b), respectively. By "best", we mean the maximal difference, between the numbers of truly detected (true positive) and falsely detected (false positive) blocks, can be achieved through adjusting the threshold  $\eta$ . To identify the forgeries, every image in question is divided into  $64 \times 64$  pixels sized blocks, each of which is labeled by a number (as the blue number shown in the center of each block). The blocks detected as contrast enhanced are highlighted in red squares. As illustrated in Figure 8, two types of incorrect classifications occur in both algorithms to be compared. The false positive error is caused by the fact that the size is too small for some blocks to guarantee the smoothness of the histogram, as a result they are recognized as enhanced ones.

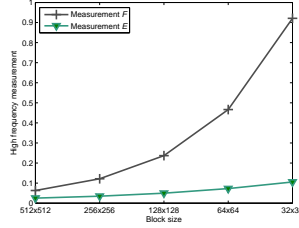


Figure 4: Average high-frequency measurement of unaltered images

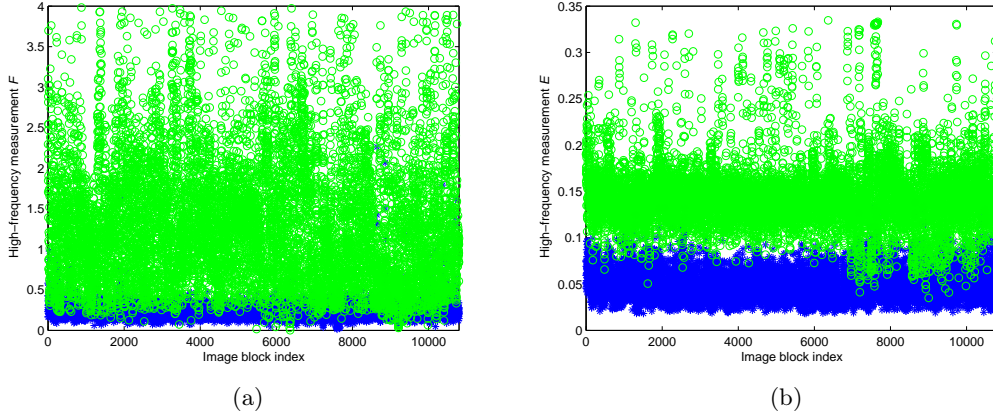


Figure 5: Scatter plots of  $F$  and  $E$  for original (blue asterisks) and  $\gamma$ -correction enhanced (green circles) image blocks sized  $128 \times 128$  pixels. (a) Stamm’s algorithm,<sup>1</sup>  $\gamma = 1.5$ , (b) improved method,  $\gamma = 1.5$ .

In the mean time, the pixel values of some blocks are likely to concentrate mainly in one or several intervals, where some peaks arise in the histogram. If these intervals coincidentally lie in the approximately linear segments of the contrast transform function (such as the middle section of the curve in Figure 7 (d)), the peaks of the original histogram are almost entirely shifted to another position of the transformed histogram. Because those peaks account for most of the pixels, this entire-peaks shift would not produce too many high-frequency traces in the histogram spectrum, resulting in the false negative errors. But both errors are reduced in the improved algorithm because of the reasons mentioned in the last part of Section 2.1. These detection results are consistent with the trend reflected in the scatter plots and ROC curves.

### 3.3 Improvement over Lin et al’s Method<sup>4</sup>

Figure 9 shows the comparison between the constant and linear threshold on  $\gamma$ -correction enhanced images. For the linear threshold method, the ROC curves are obtained by setting  $b$  to be 0.4 and changing  $a$  from 0 to 1 by 0.01. It works for most cases by setting  $b$  to be 0.4, which means that it will not increase the difficulty of searching for the optimal threshold because only  $a$  is to be determined. In consequence, the thresholds are no less than 0.4 because  $\overline{D}$  is a non-negative variable. That is the reason why the cyan curve stops at some point and will not reach to the point of  $P_{FA} = 1$ . As illustrated in Figure 9, the detection method in [4] is effective for small blocks even sized  $32 \times 32$ . For  $\gamma = 0.5$  and  $\gamma = 0.8$ , with a  $P_{FA}$  of less than 5%, our method achieves a  $P_D$  of above 90% using  $64 \times 64$  and  $32 \times 32$  pixels blocks. Actually the performance of inter-channel high-frequency similarity based method depends on how much high-frequency information one block contains rather than the block sizes. From the ROC curves, the linear threshold strategy indeed reduces the false positive rate since the false increase of  $S$  caused by image content is alleviated by incorporating  $\overline{D}$  in the threshold  $\tau$ . In the examples of real cut-and-paste image forgery detections in Figure 10, we can see that some all-black or all-white blocks are still missed, because they do not contain enough high-frequency information. However, it can be clearly seen that some blocks falsely classified as enhanced are corrected by linear threshold strategy.

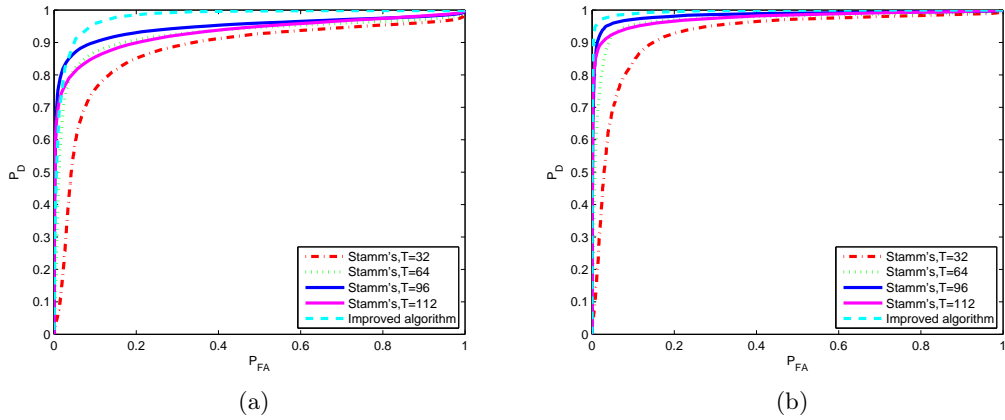


Figure 6: Detection ROC curves for images altered by  $\gamma$  correction. (a)  $\gamma = 1.5$ , blocksize= $64 \times 64$ , (b)  $\gamma = 1.5$ , blocksize= $128 \times 128$ .



Figure 7: Cut-and-paste image forgery using Photoshop. (a) The original image from which an object is cut, (b) the original image onto which the cut object is pasted, (c) the composite image and (d) parameters of Photoshop Curve Tools.

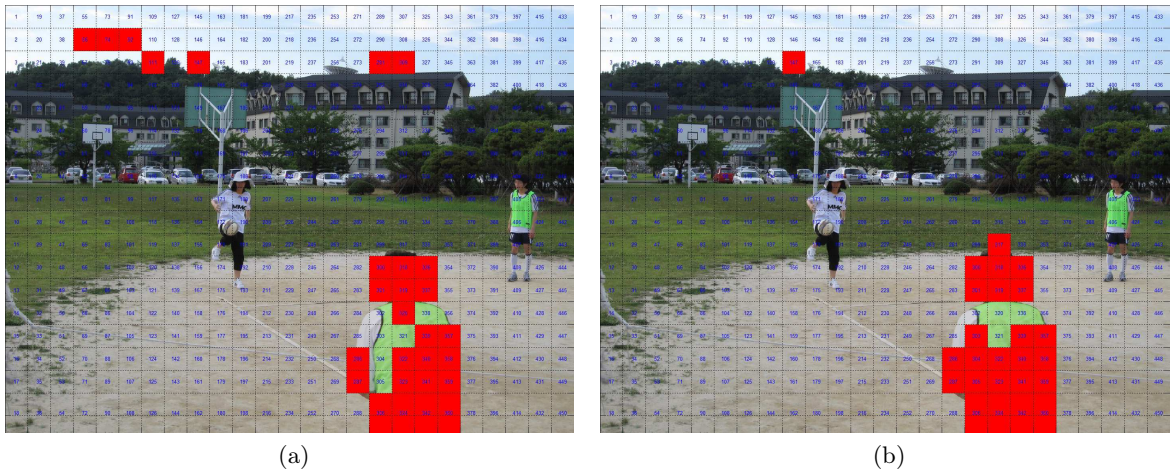


Figure 8: Detection results comparison on  $64 \times 64$  pixels blocks. (a) Using Stamm's algorithm, and (b) using improved algorithm.



## 4. SUMMARY

In this paper, we present two improved forensic methods to expose cut-and-paste image forgery by detecting contrast enhancement. For the first method, we use a new high-frequency measurement  $E$  to avoid searching for the cut-off frequency  $T$  and make it invariant to image sizes and content. For the second algorithm, we apply a soft-threshold method by modeling the relationship between the inter-channel high-frequency similarity  $S$  and the mean of the diagonal-band wavelet coefficients  $\overline{D}$ . Compared with the original algorithms in<sup>1</sup> and,<sup>4</sup> the proposed methods achieve better performance in terms of ROC curves and real cut-and-paste image forgeries. The two proposed methods are not intended for competition against each other, but for improving the two previous works [1,4] such that, in our future work, a potential fusion of these two proposed algorithms can be incorporated into an unified framework. From the detection results in Figure 8 and Figure 10, most areas missed by one proposed method are fortunately detected by the other one. So we believe that incorporating these two algorithms would be feasible and promising. However, both algorithms suffer from poor robustness against JPEG compression. So discovering specific effects of JPEG compression on the histogram and choosing wavelet coefficients that are less affected by image compression would be the other two main lines of our future work.

## REFERENCES

1. Stamm, M. and Liu, K., "Forensic detection of image manipulation using statistical intrinsic fingerprints," *IEEE Transactions on Information Forensics and Security* **5**, 492–506 (Sept. 2010).
2. Cao, G., Zhao, Y., Ni, R., and Tian, H., "Anti-forensics of contrast enhancement in digital images," *Proceedings of the 12th ACM Workshop on Multimedia and Security*, 25–34 (2010).
3. Barni, M., Fontani, M., and Tondi, B., "A universal technique to hide traces of histogram-based image manipulations," *Proceedings of the 14th ACM Workshop on Multimedia and Security*, 97–104 (2012).
4. Lin, X., Li, C.-T., and Hu, Y., "Exposing image forgery through the detection of contrast enhancement," *Proceedings of IEEE International Conference on Image Processing, Melbourne, Australia* (Sept. 2013).
5. Healey, G. and Kondepudy, R., "Radiometric ccd camera calibration and noise estimation," *IEEE Transactions on Pattern Analysis and Machine Intelligence* **16**(3), 267–276 (1994).
6. Pekkucuksen, I. and Altunbasak, Y., "Edge strength filter based color filter array interpolation," *IEEE Transactions on Image Processing* **21**(1), 393–397 (2012).
7. Hamilton Jr, J. F. and Adams Jr, J. E., "Adaptive color plan interpolation in single sensor color electronic camera," (May 13 1997). US Patent 5,629,734.
8. Gunturk, B. K., Glotzbach, J., Altunbasak, Y., Schafer, R. W., and Mersereau, R. M., "Demosaicking: color filter array interpolation in single-chip digital cameras," *IEEE Signal Processing Magazine* **22**(1), 44–54 (2005).
9. Lian, N.-X., Chang, L., Tan, Y.-P., and Zagorodnov, V., "Adaptive filtering for color filter array demosaicking," *IEEE Transactions on Image Processing* **16**(10), 2515–2525 (2007).
10. Lian, N.-X., Zagorodnov, V., and Tan, Y.-P., "Edge-preserving image denoising via optimal color space projection," *IEEE Transactions on Image Processing* **15**(9), 2575–2587 (2006).

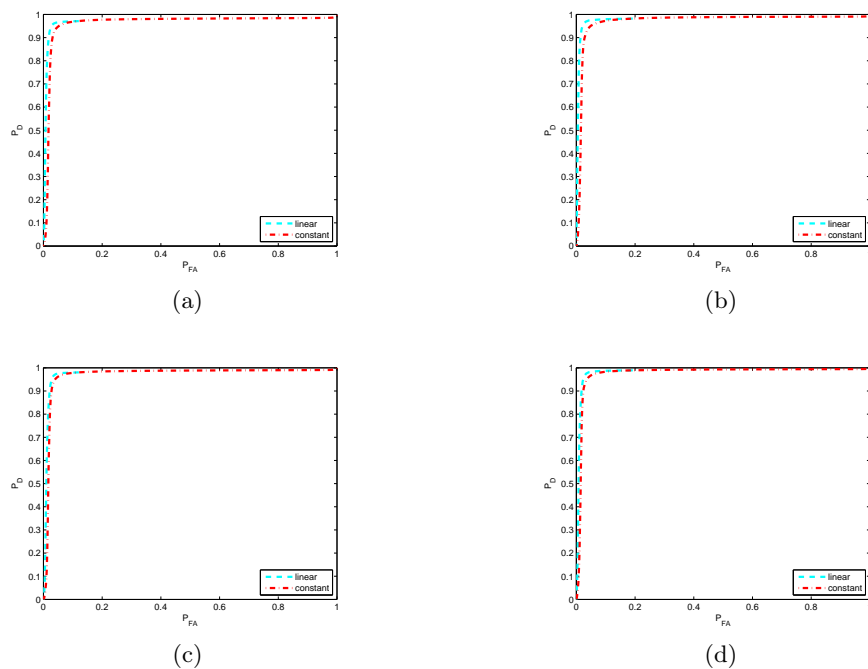


Figure 9: Performance comparison between linear and constant threshold for (a)  $\gamma = 0.5$ , blocksize= $32 \times 32$ , (b)  $\gamma = 0.5$ , blocksize= $64 \times 64$ , (c)  $\gamma = 0.8$ , blocksize= $32 \times 32$ , (d)  $\gamma = 0.8$ , blocksize= $64 \times 64$ .

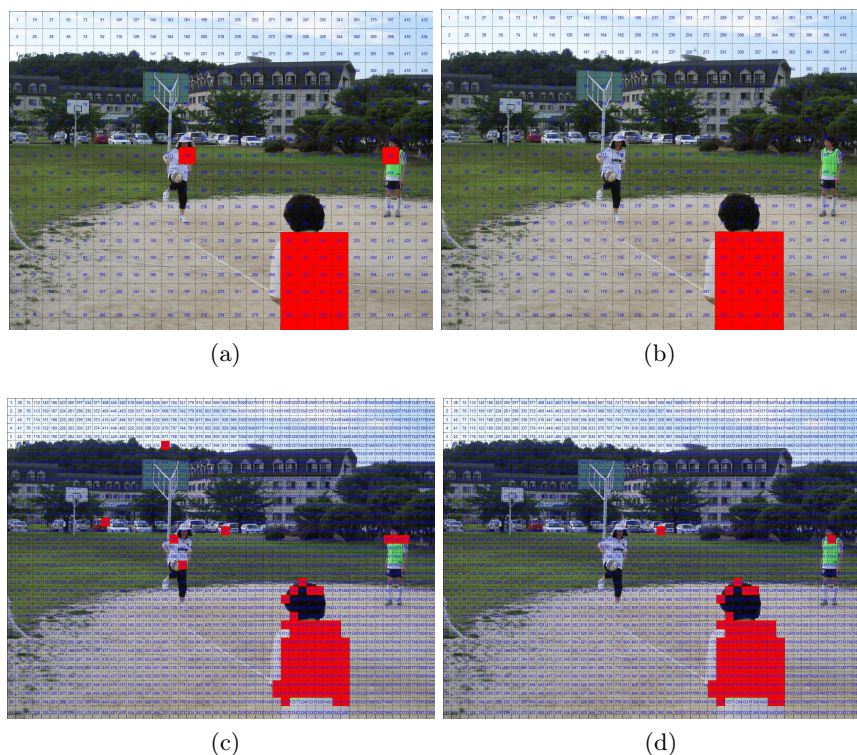


Figure 10: Detection results comparison between linear and constant threshold strategy. (a) Using linear threshold on  $64 \times 64$  pixels blocks, (b) using constant threshold on  $64 \times 64$  pixels blocks, (c) using linear threshold on  $32 \times 32$  pixels blocks, and (d) using constant threshold on  $32 \times 32$  pixels blocks.